Journal of
Instrumentation

TECHNICAL REPORT • OPEN ACCESS

Characterization of a permanent magnetic dipolar system for the FOOT experiment

Published by IOP Publishing for Sissa Medialab

Received: *June 3, 2025*
Revised: *August 29, 2025*
Accepted: *September 10, 2025*
Published: *September 30, 2025*

TECHNICAL REPORT

Characterization of a permanent magnetic dipolar system for the FOOT experiment

The FOOT collaboration

Antonio Trigilio, Lucia Sabbatini et al.

Full author list at the end of the paper

E-mail: antonio.trigilio@lnf.infn.it

Abstract: The FOOT (FragmentatiOn Of Target) experiment aims to measure double differential fragmentation cross-sections for applications in Particle Therapy and space radiation protection. A critical component of the apparatus is its magnetic spectrometer, composed of two Halbach-configured dipole magnets (M1 and M2) using NdFeB permanent magnets, designed for high field uniformity and stability. A full 3D magnetic model was developed using the OPERA solver, incorporating detailed *BH* curves and a refined meshing strategy to ensure precision along the beam axis. The resulting field map, essential for Monte Carlo simulations in FLUKA, was validated through high-resolution magnetic measurements along the longitudinal and radial axes using a Hall probe. The comparison revealed agreement within 1.4% over most of the field region. Radial scans confirmed uniformity within 1% up to 10 mm from the axis, with minor misalignments attributed to mechanical tolerances. These results confirm the accuracy of the magnetic model and its suitability for precise momentum reconstruction in the FOOT spectrometer.

Keywords: Acceleration cavities and superconducting magnets (high-temperature superconductor, radiation hardened magnets, normal-conducting, permanent magnet devices, wigglers and undulators); Beam-line instrumentation (beam position and profile monitors, beam-intensity monitors, bunch length monitors); Simulation methods and programs

https://doi.org/10.1088/1748-0221/20/09/T09010

2025 JINST 20 T09010

Contents

1 Introduction

Applied nuclear physics is a field which is growing in importance in our present times, from the possibilities opened in cancer treatment by Particle Therapy (PT), to the increasingly urgent issue of Radio Protection in Space (RPS) for short- and long-term missions. The knowledge of the interactions of protons and heavier ions with matter, including human tissues, is a key ingredient for these applications, particularly in the kinetic energy range between 100 and 800 MeV/u, of interest for medicine and radiobiology. Currently, however, the cross sections of many processes, especially nuclear fragmentation, are either missing or affected by large uncertainties due to the lack of experimental data; this limits, for example, the reliability of dose calculation in the planning of PT treatments, and the efficiency in the development of shielding for astronauts and equipment [1, 2]. Over the past 20 years, the significant interest and social impact of these applications have prompted the scientific community to renew their efforts in measuring the necessary nuclear cross sections using modern experimental setups, and have led to the accomplishment of a number of key measurements, while others still require dedicated campaigns.

Within this context, the FragmentatiOn Of Target (FOOT) collaboration aims at developing a system able to improve the understanding of double differential fragmentation cross-sections associated with the nuclear interactions of protons and heavier ions with matter, within the energy range relevant to PT and RPS applications [3]. As initial framework of investigation, the FOOT collaboration is focused on the fragmentation processes induced by protons on target during PT treatment sessions. The basic strategy involves delivering the fragments most frequently encountered (O and C atoms, which constitutes two of the main elements in the human body) to a hydrogen enriched material,

2025 JINST 20 T09010

and obtaining the cross section of interest by means of inverse kinematics through a relativistic transformation. Simultaneously, FOOT will measure the direct double differential fragmentation cross sections of light ions, such as ^{4}He, ^{16}O, and ^{12}C, interacting with targets like C, polyethylene (C_2H_4) and polymethyl methacrylate (PMMA, $C_5O_2H_8$), particularly valuable as they play a crucial role in the planning of PT treatments using ^{12}C and ^{16}O [3].

To conduct these measurements, the FOOT collaboration is building a setup that includes several components: a scintillator system [4] for ΔE-TOF measurements, ion counting and fragment identification [5]; a drift chamber for monitoring of the beam direction [6]; a magnetic spectrometer composed of pixel and strip silicon detectors paired with permanent magnets to reconstruct the momentum of fragments [7, 8]; and a calorimeter to measure the energy of the fragments [9, 10]. In addition, large-angle interactions will be analyzed using emulsion chambers, which will serve as active targets and detectors [11]. Some preliminary measurements have been already performed without the tracking detector, and results can be found in other sources [5, 12].

Since the reliability of the reconstruction of the momentum is inextricably connected to the accuracy with which the characteristics of the magnetic field are known over the whole volume of interest, we performed a detailed characterization of the bending dipolar system used in the magnetic spectrometer section. This set of measurements is essential for two fundamental reasons: first of all, it represents a validation of the initial model of the magnetic field, verifying that the experimental values of the peak fields and field quality are in agreement with the expected ones by design; secondly, it is a key point to refine and benchmark the electromagnetic simulation which has been used to extract the mapping of the magnetic field in 3D. This detailed description of the field values in space has been subsequently implemented in the FLUKA Monte-Carlo code used to evaluate the resolution and efficiency of the spectrometer in the various cases of fragments with different Z and momentum.

In this contribution, we present the work that has been undertaken to design the magnetic system, evaluate its expected performances in terms of magnetic field characteristics by means of a finite element analysis, and assess their level of agreement with the measurements performed at the National Laboratory of Frascati (LNF) of the National Institute for Nuclear Physics (INFN).

2 The magnetic system

The work on the magnets began with a magnetic preliminary design carried out by INFN-LNF, which resulted in a document outlining the technical specifications needed to achieve the scientific objectives of the project. The fabrication of the magnetic system was awarded to SigmaPhi,[1] company specialized in the production of magnets for particle accelerators and experiments, with whom INFN has had a long-standing and successful collaboration. Given the complexity of the item to be produced, a deep follow-up was done by INFN for all the project phases: from the first design review up to the final production. In all these phases the compatibility of the magnetic system with the rest of the experimental apparatus was done.

The magnetic system, as designed and manufactured, consists of two dipoles, named M1 and M2, whose main characteristics are listed in table 1. The system also includes the mechanical support required to hold the magnets in place against their repulsive force and to adjust the relative position between the two magnets.

[1]Website of SigmaPhi: https://www.sigmaphi.fr/.

2025 JINST 20 T09010

Table 1. Main characteristics of the magnetic system developed for the FOOT experiment (measured values of the final components).

Parameter	Value (M1)	Value (M2)
Nominal field (T)	1.31	0.87
Integrated field (T·mm)	170.57	152.05
Mechanical length (mm)	102	102
Effective length (mm)	130.21	174.68
Bore radius (mm)	25	53
Good Field Region radius (mm)	19	19
External radius (mm)	149	225
Transverse field homogeneity dB/B_0	2.73×10^{-2}	1.40×10^{-2}

The magnetic simulations were performed with OPERA solver[2] by both SigmaPhi and INFN for verification of calculation accuracy, and cross-checking of the results.

The two dipoles are made of NdFeB permanent magnet blocks displaced in a 12-sector Halbach configuration, with the orientations reported in figure 1. Specifically, adopting a polar coordinate system, the magnetization vector M of each block in order to obtain a dipole field can be written as:

$$\vec{M} = M_r \left[\cos\left(\varphi - \frac{\pi}{2}\right)\hat{\rho} + \sin\left(\varphi - \frac{\pi}{2}\right)\hat{\varphi} \right]$$

where $\hat{\rho}$ and $\hat{\varphi}$ are mutually orthogonal unit vectors oriented along the radial and polar directions, and M_r is the magnetization module, or residual field. The angular position φ of a single block is the one of its center of mass with respect to the horizontal plane. The magnetization vector of each magnet is, by design, the same over its whole volume in module and direction.

Each of the two dipoles is composed of multiple layers of blocks, specifically 2 layers for M1 and 3 layers for M2. The different colors in figure 1 correspond to different grades of the permanent magnet material. For both magnets, the inner layer is made of N48H, and the outer layers are made of N38UH. The choice of the grade is based on the magnetic properties (mainly the level of residual field, set by manufacturing at 13 205.9 G for N48H and 12 017.7 G for N38UH), on mechanical properties, and on commercial factors, such as availability and cost.

For each magnet, the permanent magnet blocks are housed in an aluminum case to avoid altering the magnetic field while providing the necessary mechanical structure to retain the forces acting between blocks. The thickness of the aluminum between the blocks has been minimized to maximize the amount of magnetic material, which is essential to meet the peak field and integrated value requirements. This cell configuration is completed with two plates designed to close the cells preventing longitudinal movements of the blocks and their accidental damage. The assembly is shown in figure 2.

3 Magnetic simulations

The OPERA 3D solver allows to evaluate the magnetic field configuration in the whole three-dimensional space as a set of values given on a tetrahedral meshed configuration across a series of

[2]Website of the OPERA software, 2022: https://www.3ds.com/products-services/simulia/products/opera/.

2025 JINST 20 T09010

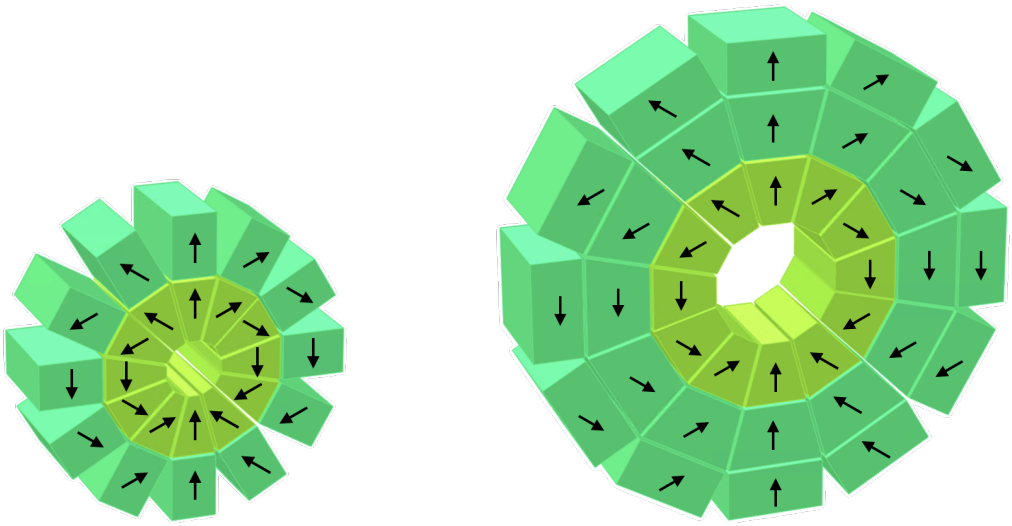

(a) M1 dipole.

(b) M2 dipole.

Figure 1. Model of the two dipoles of the FOOT magnet system as built in OPERA 3D viewer, where the orientation of the magnetic field is drawn to represent the Halbach array periodicity, resulting in the dipole configuration.

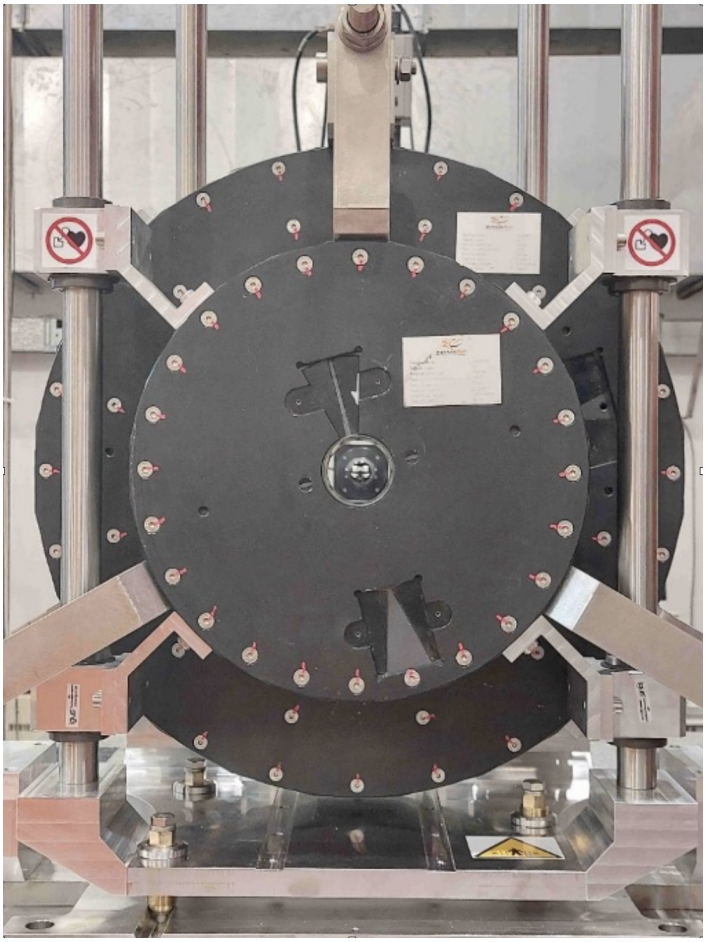

Figure 2. Dipole system assembly positioned on the magnetic measurements bench.

2025 JINST 20 T09010

nodes. The nodes displacement has been carefully studied in order to increase the sensitivity on the axis of the dipoles, where the set of measurements validating the field homogeneity is expected to take place. For this reason, the mesh has been set so that a series of equally spaced nodes, each at distance of 2 mm from the neighbors, lies on the main magnetic axis; the mesh then becomes gradually broader as it progresses towards the external boundaries of the dipoles, where the number of particles interacting with the field is expected to decrease with the radial distance. Finally, an external cylinder of air encompassing the system (radius 2.4 times the radius of the bigger magnet) acts as background.

The overall length (in the beam direction) of evaluation of the fields has been chosen to cover the whole expected region of interest, up until the zone where the value of the magnetic flux drops below 1‰ of the maximum, which corresponds to a length of 1 m taking the midpoint of the two dipoles as the center. The distance between the M1 and M2 centers is set at 16.7 cm, according to the design of the apparatus.

The permanent magnets were modeled using the BH curves of N38UH and N48H from Arnold Magnetic Technologies catalog,[3] reported in figure 3, considering a room temperature of 20°C, and the material between blocks was put to air in order to simplify the simulation, as the single cases are not expected to give a sensible contribution. Their direction of magnetization has been set according to the original project, as a standard Halbach array in dipole configuration. No time-dependent phenomena are analyzed as there are no electrical properties to consider.

The simulation generates a spatial mapping of the magnetic field, which is essential for reconstructing events in the FLUKA Monte Carlo model of the FOOT magnetic spectrometer. The estimated field has been validated through a series of measurements conducted along specific axes, which will be detailed in the following section.

4 Magnetic measurements

For the following section, the reference system will be the one portrayed in figure 4, centered at the midpoint of the two dipoles M1 and M2. For the coordinates, we will refer to z as the longitudinal, to x as the horizontal and to y as the vertical.

Before installment of the dipole system in the LNF Magnetic Measurements Laboratory, SigmaPhi performed a characterization of the individual magnets M1 and M2 and of the final assembly with point-like measurements of the magnetic field component directed along the y axis (B_y). In particular, 5 longitudinal scans were performed with a single axis Hall probe positioned on a motorized holder capable of translation along the 3 axis, moving on a path parallel to the z axis, and measuring the values of B_y with step $\Delta z = 5$ mm, in a z range of ±600 mm. The horizontal position of the 5 scans was varied at $x = 0$ mm,±10 mm and ±19 mm.

A further measurement campaign, decreasing the step Δz at 2 mm, was performed at LNF with a similar single axis Hall probe, powered and read by a teslameter with sensitivity ±0.5 G, and mounted on a translating holder with positioning accuracy of ±10 µm, installed on a concrete bench to minimize the oscillations due to the probe translations. Due to the dimensions of the mechanical arm holding the probe, the maximum z coordinate depends on the x coordinate at which the scan is performed. Also, to allow a more extended exploration, the disposition of the magnets is switched with respect to their operation, so the probe enters M2 first and subsequently M1.

[3] Neodymium Iron Boron Product Catalog: https://www.arnoldmagnetics.com/resources/technical-publications/.

2025 JINST 20 T09010

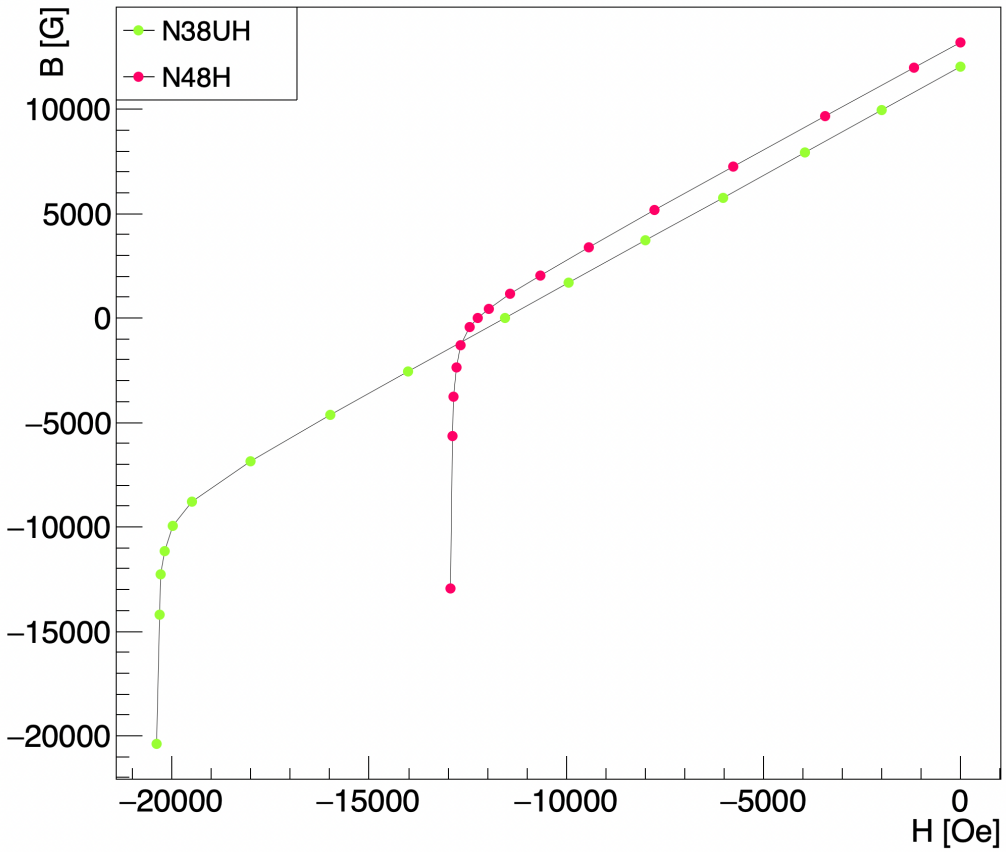

Figure 3. *BH* curves for the permanent magnets N38UH and N48H, taken from Arnold Magnetic Technologies, implemented in the simulation.

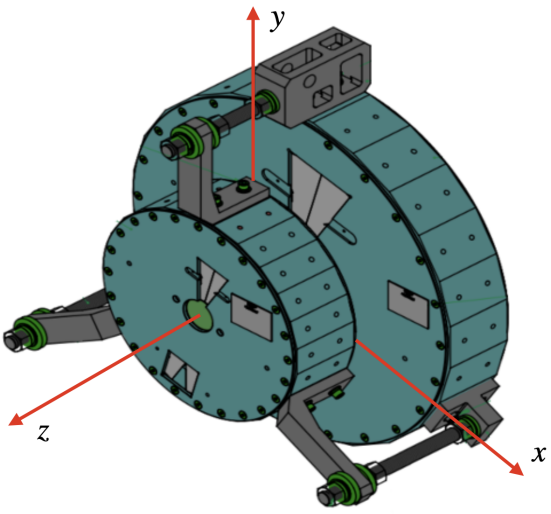

Figure 4. Reference coordinate system used for the magnetic measurements.

2025 JINST 20 T09010

The following longitudinal scans have been performed:

- preliminary scan with step $\Delta z = 5$ mm to determine the position of the peaks and measure the center of our reference frame $(x, y, z) = (0, 0, 0)$ at the midpoint of the two dipoles;
- 2 radial scans performed at the position of the peaks on M1 and M2, with step $\Delta x = 1$ mm, x range ± 19 mm;
- 5 longitudinal scans with $\Delta z = 2$ mm, z range from -465 mm to 499 mm, taken at $x = 0, \pm 4$ mm, ± 8 mm;
- 2 longitudinal scans with $\Delta z = 2$ mm, z range from -465 mm to 299 mm, taken at $x = \pm 10$ mm;
- 2 longitudinal scans with $\Delta z = 2$ mm, z range from -465 mm to 17 mm, taken at $x = \pm 19$ mm.

5 Comparison between measurements and simulations

In this section, we report the results of the magnetic measurements and experimental benchmark of the 3D model for the magnet system. The analyses are focused on the trend of the magnetic field as a function of the longitudinal coordinate z at different horizontal positions x. We first evaluate the agreement between simulations and measurements showing the relative difference between data at each position measured. We also show the agreement in terms of the magnetic parameters such as the maximum field of the two dipoles and the integral field, and investigate possible sources of discrepancies and errors.

5.1 Longitudinal scan: central axis

For a first evaluation, figure 5 shows the agreement between the simulated and measured longitudinal profile of the magnetic flux of the FOOT dipoles system. By performing a raw interpolation of the points, we see that the peaks lie symmetrically with respect to the center at about ± 80 mm. The curve is the result of the superposition of the fields by the two arrays, which is responsible for the asymmetric tails.

5.2 Radial scans: uniformity evaluation

In terms of the field uniformity, we took the values measured by SigmaPhi of the field at different positions along x and compared them with the results of our own radial scans. Figure 6 shows the comparison between radial measurements, highlighting the field uniformity which stays within 1% of relative difference with respect to the value at the center of the dipole up to 10 mm for M1, and is even better for M2, reaching 1% at about 20 mm due to the larger bore. The radial scan also shows a slight misalignment of 0.5 mm between the mechanical axes of the two magnets in the final system that was delivered to LNF; the deviation can be seen from the different position of the minima (denoted as x_{min}) on the radial scans, extrapolated from a parabolic fit of the LNF measurements, and from the asymmetry with respect to $x = 0$ in the M1 profile (figure 6(a)). The sources of this difference lie on the mechanical positioning error and on the intensity and direction of magnetic remanence. Thanks to this magnetic characterization it would be possible to align the two magnetic axes or to take into account this mismatch in the reconstruction algorithm.

2025 JINST 20 T09010

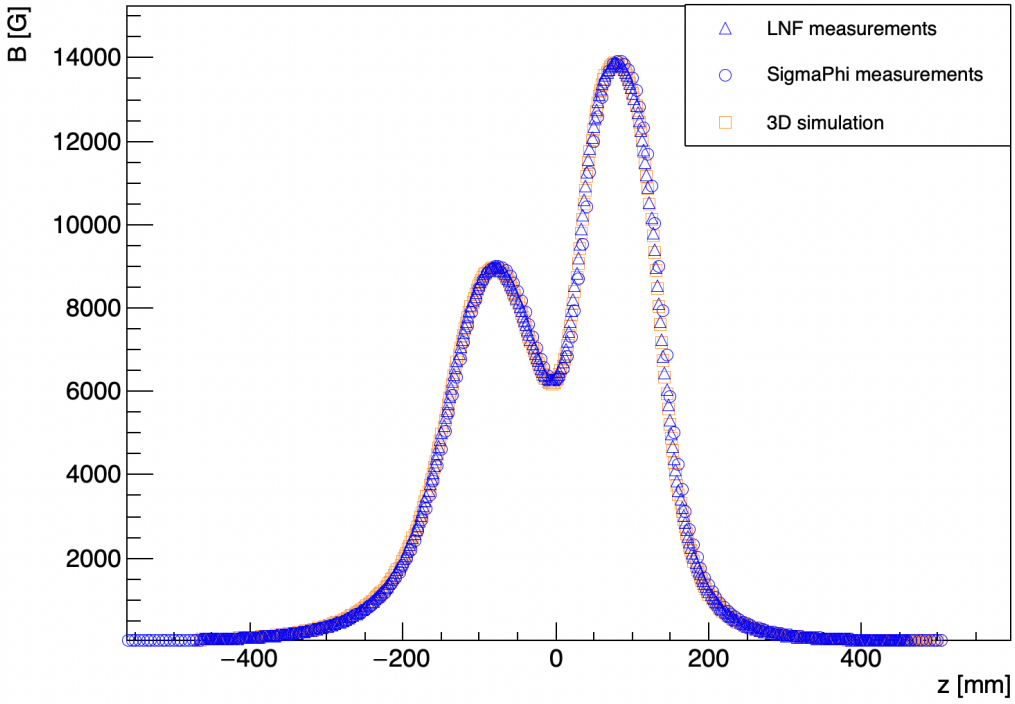

Figure 5. Magnetic field of the FOOT dipoles system evaluated on a longitudinal scan passing through the mechanical centers of the dipoles. The experimental points (in blue), taken by the manufacturer SigmaPhi and by the LNF magnetic measurement laboratory, are compared with the results of the OPERA 3D simulation (in orange).

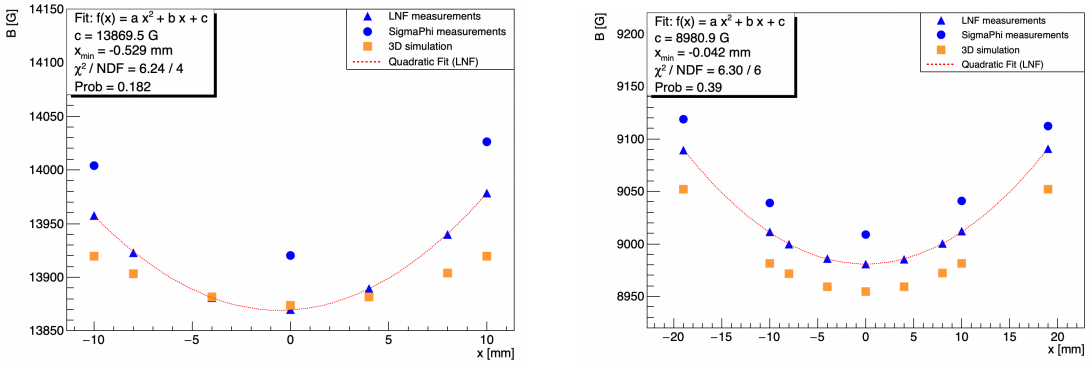

(a) Radial scan at $z = -80$ mm (M1 peak).

(b) Radial scan at $z = 80$ mm (M2 peak).

Figure 6. Radial positions evaluation. Error bars are not visible due to the high sensitivity of the experimental setup, as reported in section 4. A parabolic fit is used to determine the position of the minima, denoted as x_{min}. The small relative differences between the two experimental measurements and the simulations, which are not visible in figure 5 (being orders of magnitude less than B_{max}) can be appreciated due to the zoomed-in interval in the B axis.

5.3 Table of comparison

Table 2 shows a comparison between four values of merit taken from the initial SigmaPhi characterization, measurement performed at LNF and the results of the OPERA simulation: the values of the magnetic field at $z = (-5, \pm 80\,\text{mm})$ (corresponding respectively to the points at which the local minimum and the two local maxima of B_y are found) and the integrated field measured at the longest common interval between measurements taken by SigmaPhi and LNF, which, for reasons of limitation of the measurements along z due to the maximum reach of the probe inside the magnet, is not the physical integral value of the field.

The relative difference between the two values B_y^A and B_y^B obtained with two methods (denoted as $\Delta B_y/B_y$ for A–B) is computed as $(B_y^A - B_y^B)/B_y^B$.

5.4 Longitudinal scan analysis: $x = 0$

Figure 7 shows the relative differences $(B_y^{\text{sim}} - B_y^{\text{meas}})/B_y^{\text{meas}}$ (which we will refer to as $\Delta B_y/B_y$ for brevity) between the simulations and the measurements of each longitudinal scan performed at different x (in this case, for simplicity, we only compare LNF measurements with the 3D model). In the interest of clarity, we restrict the interval between $z = \pm 300\,\text{mm}$, because the low values of B_y far from the core of the magnet causes the relative error to diverge at higher distances, even if the absolute difference is small, and generally we are more interested in the errors in the region that contribute more to the integral field.

We can see that there are regular oscillations of $\Delta B_y/B_y$ that can have various origins in the magnet actual geometry. Overall, the simulation slightly underestimates the actual field. The highest discrepancy is observed at $z = 200\,\text{mm}$, corresponding to the tail of the M1 distribution (see figure 5), where the relative difference is -3.8% and B_y measures 1200 G. The difference progressively shifts towards higher values for values of $z > 280\,\text{mm}$, where the field magnitude becomes negligibly small.

For $z < 140\,\text{mm}$, the agreement is remarkably satisfied, with a maximum absolute value of $\Delta B_y/B_y$ at 1.4% and reaching local minima at the location of the peaks, mirroring the geometry of the spectrometer dipoles; in fact, in the two points at $x = \pm 80\,\text{mm}$, the magnetic field reaches local maxima, and therefore the relative error, provided the simulated field approximates well the actual one, becomes negligibly small. Consequently, the simulation exhibits high accuracy at these extrema, and is validated by the measurements.

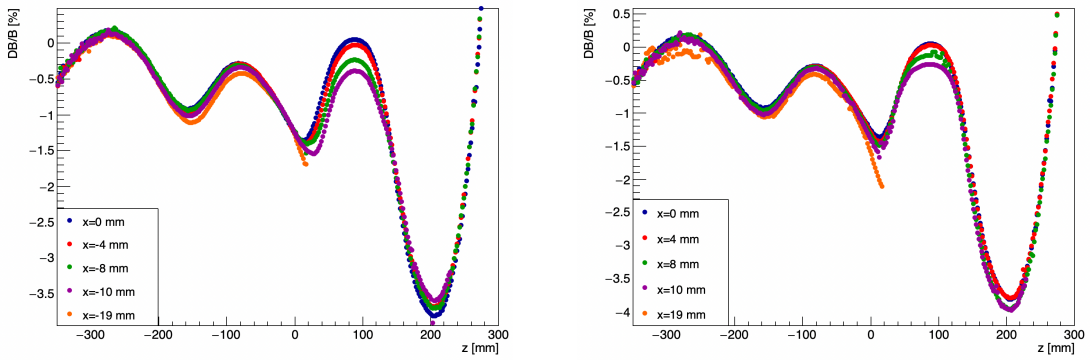

(a) x negative.

(b) x positive.

Figure 7. Relative difference for longitudinal scans performed at different horizontal coordinates x, represented by points of different colors, between values of B_y computed by OPERA 3D simulations and measurements at LNF.

2025 JINST 20 T09010

5.5 Sources of errors

To conclude our analysis, we explored the effects due to the misplacement or misalignment of the dipoles that could contribute errors to the field modeling. We already saw, from the radial scan analysis, that the variation on a small interval (about ±1 mm) around the peaks of the distribution of $\Delta B_y/B_y$ is less than 0.1%, so we expect that a shift in the horizontal direction x of one of the two magnets does not give a sensible effect on the evaluation of the field by the model. We nevertheless performed 4 additional runs of simulation varying translating rigidly the M1 magnet of 1 mm or 2 mm to the left and to the right. The results, shown in figure 8, where we plotted the relative difference between the simulation performed with M1 on axis and the others with M1 off-axis, confirm our initial hypothesis; the difference between the initial simulation and the others is too small (less than 0.3%) to account for any possible correction of geometry effects.

The second possibility is a translation in the z direction varying the distance between M1 and M2 at a maximum of ±1 mm. Figure 9 shows the result in terms of $\Delta B_y/B_y$ varying this parameter around the nominal distance of 167 mm. It can be seen that the distributions all give satisfying results at the centers of the two magnets, but at larger distances the model which we adopted is still the one that gives the smaller errors, and the smaller integral of the distribution in absolute value.

Furthermore, we performed tests introducing an initial angle between the axes of the magnets, for example rotating M1 around the vertical axis of and angle θ of 5 mrad, which is the resolution at which the two magnets are supposed to be aligned. Figure 10 shows the difference between the longitudinal profile obtained with the axes of the magnets coinciding and the one with a tilt of 5 mrad, which, being lower than 0.1% in absolute value, is understood as negligible.

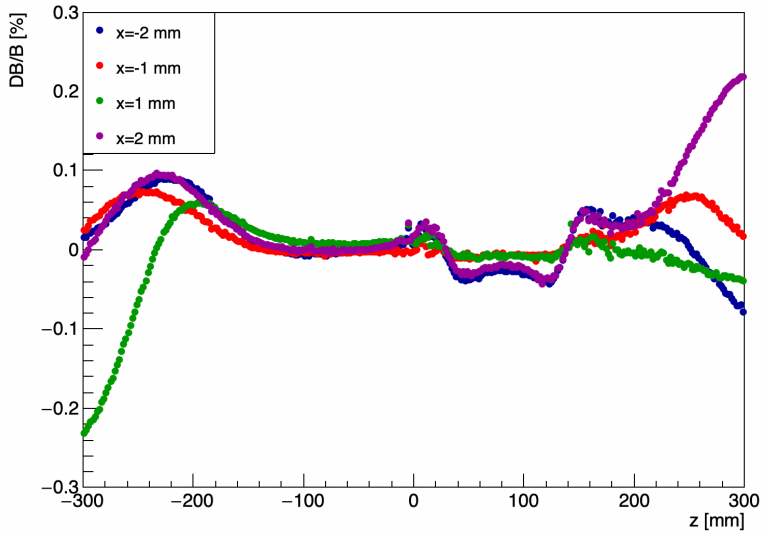

Figure 8. Relative difference between the values of B_y obtained from different simulations introducing an error from displacement of M1 in x and the reference one ($x = 0$).

6 Conclusions

The experimental characterization of the magnet system for the FOOT detector has given convincing results that the magnet satisfies the requirements needed in terms of field integral and uniformity. In

Table 2. Summary of main parameters from measurements and simulation. The columns gather data taken at different horizontal positions x. Each x is associated with an interval of integration along z due to mechanical constraints. The values of B_y reported are taken at the two magnets centers positions ($z = \pm 80$ mm) and at the local minimum ($z = -5$ mm). $\Delta B_y/B_y$ is the relative difference between experimental values obtained by LNF and SigmaPhi in one row, and between the value obtained from simulation and measured by LNF in the other. Homogeneity is computed as the percentage difference between B_y taken at a certain x and at $x = 0$. The values of integrated field and the relative differences between experimental and simulated values are computed along the interval of integration specific for an x-coordinate longitudinal scan.

	Interval of integration:	$x = -19$ mm ($z = [-465; 17]$ mm)	$x = -10$ mm ($z = [-465; 229]$ mm)	$x = 0$ mm ($z = [-465; 499]$ mm)	$x = 10$ mm ($z = [-465; 229]$ mm)	$x = 19$ mm ($z = [-465; 17]$ mm)
M1 peak ($z = -80$ mm)						
B_y (G)	SigmaPhi	14269	14004	13920	14026	14256
	LNF	—	13954	13867	13974	—
	Sim	—	13919	13874	13919	—
$\Delta B_y/B_y$ (%)	LNF–SigmaPhi	—	–0.36	–0.38	–0.37	—
	Sim–LNF	—	–0.25	0.05	–0.39	—
Homogeneity (%)	SigmaPhi	2.51	0.60	—	0.76	2.41
	LNF	—	0.63	—	0.77	—
M2 peak ($z = 80$ mm)						
B_y (G)	SigmaPhi	9119	9039	9009	9041	9112
	LNF	9089	9011	8981	9012	9090
	Sim	9052	8982	8955	8982	9052
$\Delta B_y/B_y$ (%)	LNF–SigmaPhi	–0.33	–0.31	–0.31	–0.32	–0.24
	Sim–LNF	–0.41	–0.32	–0.29	–0.33	–0.42
Homogeneity (%)	SigmaPhi	1.22	0.33	—	0.36	1.14
	LNF	1.21	0.34	—	0.35	1.22
Local minimum ($z = -5$ mm)						
B_y (G)	SigmaPhi	6106	6223	6265	6216	6102
	LNF	6112	6223	6262	6214	6096
	Sim	6024	6142	6189	6142	6024
$\Delta B_y/B_y$ (%)	LNF–SigmaPhi	0.10	> 0.01	–0.05	–0.03	–0.11
	Sim–LNF	–1.44	–1.30	–1.17	–1.16	–1.18
Integral field (T mm)	SigmaPhi	152.23	319.39	321.99	319.67	152.21
	LNF	152.55	318.42	320.95	318.61	152.48
	Sim	151.33	315.90	318.92	315.90	151.33
$\Delta B_{\text{int}}/B_{\text{int}}$ (%)	LNF–SigmaPhi	0.21	–0.30	–0.32	–0.33	0.18
	Sim–LNF	–0.80	–0.79	–0.63	–0.85	–0.75

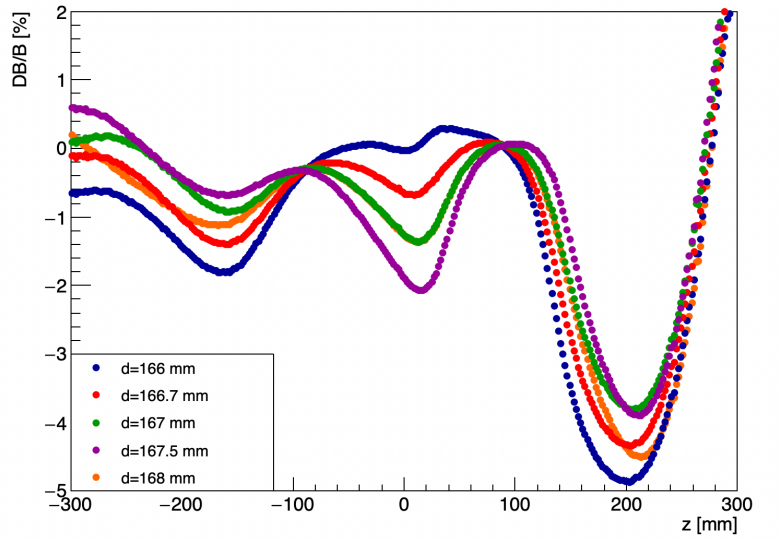

Figure 9. Relative differences for longitudinal scans performed at $x = 0$ between values of B_y computed by OPERA 3D simulations and measurements at LNF, introducing different errors from displacement in z (varying slightly the distance between M1 and M2).

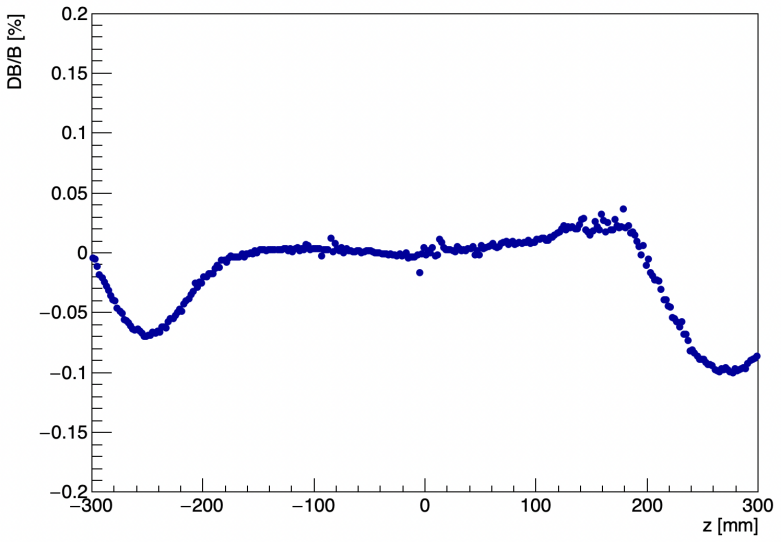

Figure 10. Relative difference between simulated longitudinal profiles obtained with the axes of the magnets coinciding and introducing an error from displacement in θ by rotating M1 of 5 mrad around the vertical axis.

addition, it has been instrumental to validate the magnetic field model implemented in the Monte Carlo simulation of the spectrometer. Further refinements are possible, although the level of agreement strongly suggests that the systematic uncertainty due to geometrical imperfections on the blocks displacement should not affect the overall resolution. Nevertheless, studies are ongoing and we refer the reader to the FOOT collaboration site[4] for regular updates.

[4]FOOT experiment website: https://web.infn.it/foot/.

2025 JINST 20 T09010

References

[1] M. Durante and H. Paganetti, *Nuclear physics in particle therapy: a review*, *Rept. Prog. Phys.* **79** (2016) 096702.

[2] S. Muraro, G. Battistoni and A.C. Kraan, *Challenges in Monte Carlo Simulations as Clinical and Research Tool in Particle Therapy: A Review*, *Front. Phys.* **8** (2020) 567800.

[3] G. Battistoni, M. Toppi and V. Patera, *Measuring the Impact of Nuclear Interaction in Particle Therapy and in Radio Protection in Space: the FOOT Experiment*, *Front. Phys.* **8** (2021) 568242.

[4] A.C. Kraan et al., *Charge identification of nuclear fragments with the FOOT Time-Of-Flight system*, *Nucl. Instrum. Meth. A* **1001** (2021) 165206.

[5] M. Toppi et al., *Elemental fragmentation cross sections for a ^{16}O beam of 400 MeV/u kinetic energy interacting with a graphite target using the FOOT ΔE-TOF detectors*, *Front. Phys.* **10** (2022) 979229.

[6] Y. Dong et al., *The Drift Chamber detector of the FOOT experiment: Performance analysis and external calibration*, *Nucl. Instrum. Meth. A* **986** (2021) 164756.

[7] G. Silvestre et al., *Characterization of 150 µm thick silicon microstrip prototype for the FOOT experiment*, 2022 *JINST* **17** P12012.

[8] Y. Dong et al., *The FLUKA Monte Carlo simulation of the magnetic spectrometer of the FOOT experiment*, *Comput. Phys. Commun.* **307** (2025) 109398.

[9] N. Bartosik et al., *Development and performance assessment of the BGO calorimeter module for the FOOT experiment*, 2025 *JINST* **20** P03021.

[10] L. Scavarda, *Design and performance of the Calorimeter for the FOOT experiment*, *Nuovo Cim. C* **43** (2020) 123.

[11] G. Galati et al., *Charge identification of fragments with the emulsion spectrometer of the FOOT experiment*, *Open Phys.* **19** (2021) 383.

[12] I. Mattei et al., *Measurement of 12C Fragmentation Cross Sections on C, O, and H in the Energy Range of Interest for Particle Therapy Applications*, *IEEE Trans. Radiat. Plasma Med. Sci.* **4** (2020) 269.

2025 JINST 20 T09010

The FOOT collaboration

Antonio Trigilio[a,*], Lucia Sabbatini[a], Andrey Alexandrov[b], Behcet Alpat[c], Giovanni Ambrosi[c], Stefano Argirò[d,e], Mattia Barbanera[c], Nazar Bartosik[e], Giuseppe Battistoni[f], Maria Giuseppina Bisogni[g,h], Vincenzo Boccia[i,b], Sergio Brambilla[f], Francesca Cavanna[e], Piergiorgio Cerello[e], Esther Ciarrocchi[h,g], Nicola D'Ambrosio[j], Angelica De Gregorio[k], Giovanni De Lellis[i,b], Antonia Di Crescenzo[i,b], Benedetto Di Ruzza[l,m], Matilde Dondi[n,o], Marco Donetti[p,e], Yunsheng Dong[f], Marco Durante[i,q], Riccardo Faccini[r,k], Veronica Ferrero[e], Christian Finck[s], Elisa Fiorina[e], Marco Francesconi[b], Matteo Franchini[o,n], Gaia Franciosini[t,k], Giuliana Galati[u,m], Luca Galli[h], Maria Ionica[c], Antonio Iuliano[b], Keida Kanxheri[c], Bharat Kharpuse[e], Aafke Christine Kraan[h], Adele Lauria[i,b], Ernesto Lopez Torres[v,e], Tommaso Maggipinto[u,m], Marco Magi[t,k], Alice Manna[n,o], Michela Marafini[w,k], Simone Masci[j], Maurizio Massa[h], Cristian Massimi[n,o], Ilaria Mattei[f], Alberto Mengarelli[n], Alessio Mereghetti[p], Riccardo Mirabelli[r,k], Andrea Moggi[h], Maria Cristina Montesi[x,b], Maria Cristina Morone[y,z], Matteo Morrocchi[h,g], Silvia Muraro[f], Nadia Pastrone[e], Vincenzo Patera[t,k], Francesco Pennazio[e], Francesca Peverini[c,aa], Claudia Pisanti[n,o], Pisana Placidi[c,ab], Marco Pullia[p], Flaminia Quattrini[r,k], Luciano Ramello[ac,e], Claire-Anne Reidel[q], Riccardo Ridolfi[n,o], Lucia Salvi[c,aa], Claudio Sanelli[a], Alessio Sarti[t,k], Osamu Sato[ad], Simone Savazzi[p], Lorenzo Scavarda[ae], Angelo Schiavi[t,k], Christoph Schuy[q], Emanuele Scifoni[af], Leonello Servoli[c], Gianluigi Silvestre[c,aa], Mario Sitta[ac,e], Benedetto Spadavecchia[d,e], Roberto Spighi[n], Eleuterio Spiriti[a], Luana Testa[r,k], Valeri Tioukov[b], Sandro Tomassini[a], Francesco Tommasino[ag,af], Marco Toppi[t,k], Giacomo Traini[k], Giacomo Ubaldi[n,o], Alessandro Valetti[e,d], Marie Vanstalle[s], Mauro Villa[o,n], Ulrich Weber[q], Roberto Zarrella[n,o], Antonio Zoccoli[n,o], Alessandro Vannozzi[a]

[a] *Istituto Nazionale di Fisica Nucleare (INFN), Laboratori Nazionali di Frascati, Frascati, Italy*
[b] *Istituto Nazionale di Fisica Nucleare (INFN), Section of Napoli, Napoli, Italy*
[c] *Istituto Nazionale di Fisica Nucleare (INFN), Section of Perugia, Perugia, Italy*
[d] *Department of Physics, University of Torino, Torino, Italy*
[e] *Istituto Nazionale di Fisica Nucleare (INFN), Section of Torino, Torino, Italy*
[f] *Istituto Nazionale di Fisica Nucleare (INFN), Section of Milano, Milano, Italy*
[g] *Department of Physics, University of Pisa, Pisa, Italy*
[h] *Istituto Nazionale di Fisica Nucleare (INFN), Section of Pisa, Pisa, Italy*
[i] *Department of Physics "E. Pancini", University of Napoli, Napoli, Italy*
[j] *Istituto Nazionale di Fisica Nucleare (INFN), Section of Gran Sasso National Laboratories, Assergi (L'Acquila), Italy*
[k] *Istituto Nazionale di Fisica Nucleare (INFN), Section of Roma 1, Rome, Italy*
[l] *University of Foggia, Foggia, Italy*
[m] *Istituto Nazionale di Fisica Nucleare (INFN), Section of Bari, Bari, Italy*
[n] *Istituto Nazionale di Fisica Nucleare (INFN), Section of Bologna, Bologna, Italy*
[o] *Department of Physics and Astronomy, University of Bologna, Bologna, Italy*
[p] *Centro Nazionale di Adroterapia Oncologica (CNAO), Pavia, Italy*
[q] *Biophysics Department, GSI Helmholtzzentrum für Schwerionenforschung, Darmstadt, Germany*
[r] *Department of Physics, University of Rome La Sapienza, Rome, Italy*
[s] *Université de Strasbourg, CNRS, IPHC UMR 7871, F-67000 Strasbourg, France*
[t] *Department of Scienze di Base e Applicate per l'Ingegneria (SBAI), University of Rome La Sapienza, Rome, Italy*
[u] *Department of Physics, University of Bari, Bari, Italy*
[v] *CEADEN, Centro de Aplicaciones Tecnologicas y Desarrollo Nuclear, Havana, Cuba*
[w] *Museo Storico della Fisica e Centro Studi e Ricerche Enrico Fermi, Rome, Italy*
[x] *Department of Chemistry, University of Napoli, Napoli, Italy*
[y] *Department of Physics, University of Rome Tor Vergata, Rome, Italy*
[z] *Istituto Nazionale di Fisica Nucleare (INFN), Section of Roma Tor Vergata, Rome, Italy*

2025 JINST 20 T09010

[aa] *Department of Physics and Geology, University of Perugia, Perugia, Italy*
[ab] *Department of Engineering, University of Perugia, Perugia, Italy*
[ac] *Department of Science and Technological Innovation, University of Piemonte Orientale, Alessandria, Italy*
[ad] *Department of Physics, Nagoya University, Nagoya, Japan*
[ae] *ALTEC, Aerospace Logistic Technology Engineering Company, Corso Marche 79, 10146 Torino, Italy*
[af] *Trento Institute for Fundamental Physics and Applications, Istituto Nazionale di Fisica Nucleare (TIFPA-INFN), Trento, Italy*
[ag] *Department of Physics, University of Trento, Trento, Italy*

[*] *Corresponding author*

2025 JINST 20 T09010